Influence of the Displacement out of the Center of Mass and Nonaxiality of the Dipole on the Thermodynamics of Liquids Composed of Linear Dipole Molecules

ARTICLE *in* THE JOURNAL OF PHYSICAL CHEMISTRY B · AUGUST 2008

Impact Factor: 3.3 · DOI: 10.1021/jp801680z · Source: PubMed

5 AUTHORS, INCLUDING:

S. Lago
Universidad Pablo de Olavide
129 PUBLICATIONS **1,747** CITATIONS
SEE PROFILE

Francisco gámez
Universidad Pablo de Olavide
36 PUBLICATIONS **189** CITATIONS
SEE PROFILE

Benito Garzón
University Foundation San Pablo CEU
28 PUBLICATIONS **300** CITATIONS
SEE PROFILE

Influence of the Displacement out of the Center of Mass and Nonaxiality of the Dipole on the Thermodynamics of Liquids Composed of Linear Dipole Molecules

S. Lago,*,† F. Gámez,† M. Cortada,† P. J. Merkling,† and B. Garzón‡

Dpt. Sistemas Físicos, Químicos y Naturales, Universidad Pablo de Olavide, Ctra. de Utrera Km. 1, Seville 41013, Spain, and Dpt. Física Aplicada, Fisicoquímica y Óptica Facultad de Farmacia, Universidad San Pablo CEU, Urb. Montepríncipe, Boadilla del Monte, 28668 Madrid, Spain

Received: February 26, 2008; Revised Manuscript Received: April 14, 2008

We present results for organic liquids modeled as linear rods with an embedded point dipole shifted from the geometrical center. Previously, we have obtained results for the vapor−liquid equilibrium (VLE) of similar systems with centered point dipoles. Our results included both models and applications to real systems. Results presented here are based on a previous work (*Phys. Rev. E* **2003**, *68*, 021201) on the structural properties of these systems where relevant results about the appearance of dimers were found. Now, we have also performed systematic simulations on these systems to calculate the VLE of models with different aspect ratios, dipole shifts, and dipole strengths using the Gibbs ensemble Monte Carlo (GEMC) to calculate equilibrium densities and vapor pressure at each temperature. The applications considered here include some important substances such as 1-amines, acetonitrile, and 1-alcohols whose intermolecular parameters were fitted from our model simulations. Furthermore, we have used quantum chemistry calculations to obtain a reliable charge distribution, and we have applied our model to predict the vapor pressure of α,ω-diols where experimental results are rather scarce. Our results show a general improvement of the agreement between experiment and models compared to centered dipole models previously used. Results for amines are particularly remarkable.

I. Introduction

Liquids composed of linear molecules bearing a dipole are ubiquitous as solvents and as important products in the chemical industry.[1,2] Most of these liquids are modeled accurately as linear rods with a point dipole embedded in the center of the rod. Indeed, a number of simulation studies providing good predictions of thermodynamic properties for this kind of liquids are well-known.[3–6] These studies are usually based on previous accurate simulations of thermodynamic properties of simple models. However, this kind of models represents poorly the shape and electronic charge distribution of important molecules where the charge distribution is not symmetric with respect to the center of the molecule or the maximum charge density region does not extend along the molecular axis. For example, it is not very likely that 1-alcohols, 1-amines, or 1-chloroalkanes can be well represented by such a symmetric model. Moreover, the dipole orientation and its modulus can change during an energy transfer process, and these changes can be analyzed experimentally or by simulations of the molecule in an excited state.[7–13] The main goal of this paper is to study in a systematic way the influence on thermodynamic properties of the displacement of a point dipole out of the geometrical center to an extreme of the molecule. Some previous results, mainly referring to the structure, have been already published, finding interesting differences among liquids with centered and noncentered dipoles.[14] We show here that relevant differences for thermodynamic properties of the models are found. The results obtained here allow for fitting in a more accurate way thermodynamic properties of relevant molecules. For instance, 1-octanol is usually employed to obtain the partition coefficient octanol−water characterizing a broad number of pharmaceutical compounds[15–17] and relevant compounds in environmental chemistry.[18–20] We have previously shown that a good knowledge of the vapor−liquid equilibrium allows for obtaining vaporization enthalpy.[4] From this enthalpy it is possible to obtain solubility factors[4] and, thence, a relative scale of partition coefficients. We show in this paper that our model based on chemical intuition gives very good results for nitrogenated compounds such as 1-amines and acetonitrile. However, we find that results are clearly worse for some 1-alcohols where discrepancies between results from simple models and experiment are usually attributed to the formation of hydrogen bonds. By more in-depth study of this explanation, we have made quantum chemical computations for the dimers of α,ω-diols proposing new models for these dimers and calculating the vapor pressure curve. Note that the appearance of dimers was pointed out in a previous paper based solely on structural results.[14] In this case, our findings seem to improve on the results considering only monomers but more experiments will be needed to be conclusive. We are aware of simulations for angular molecules with similar potentials[21,22] and theoretical results for simple mixtures,[23] but for sake of clarity, we restrict here ourselves to the simulation of linear models of pure substances. However, some interesting conclusions for mixtures can be directly obtained through Hildebrand solubility parameter as shown below. With all this information in mind, this paper is scheduled as follows: section II is devoted to present the model and the relevant simulation parameters; section III shows the results for vapor−liquid equilibrium of models in a systematic way and obtain molecular parameters for relevant organic substances such as amines, acetonitrile and long chain alcohols. Finally, some interesting remarks and conclusions are presented in section IV.

* Author to whom correspondence should be addressed: slagara@upo.es
† Universidad Pablo de Olavide.
‡ Universidad San Pablo CEU.

10.1021/jp801680z CCC: $40.75
Published on Web 06/14/2008

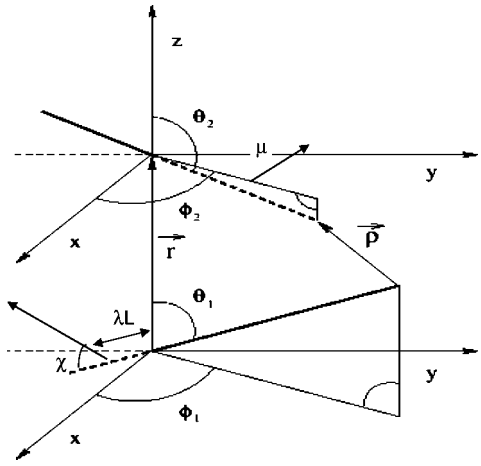

Figure 1. Potential model used in this work showing the shortest distance between two linear molecules ρ, the relative angles defining orientations and dipole interactions, and the new parameters λ and χ defined in the text.

II. Molecular Model, Simulation Conditions, and Relation to Experiment

Our molecules are represented by linear rods of length L with an embedded point dipole in some position of the rod. This dipole can be aligned or nonaligned with the rod (axial or nonaxial dipoles). The rods mutually interact according to an intermolecular pair potential given by

$$u(r,\Omega) = u^K(r,\Omega) + u^{\mu\mu}(r,\Omega) \quad (1)$$

The nonpolar intermolecular interactions are described through the Kihara potential

$$u^K = 4\varepsilon\left[\left(\frac{\sigma}{\rho}\right)^{12} - \left(\frac{\sigma}{\rho}\right)^{6}\right] \quad (2)$$

In this equation, ρ is the shortest distance between the molecular cores modeled as rods of length L (see Figure 1). ρ depends on the distance between centers of mass as well on the mutual molecular orientations, but we write ρ for simplicity. σ and ε are two parameters with dimensions of length and energy, respectively. Computation of ρ is not trivial but we have developed fast algorithms in the past[24–26] to compute it. These algorithms allow the calculation of several millions of values of ρ per second. Often, a question is raised about the efficiency of this algorithm in comparison with more popular site−site (atom−atom) intermolecular potentials. A restricted comparison was made some years ago,[27] but more recently, a complete study of site−site potentials was published by Vesely[28] studying the efficiency of site−site potentials as a function of the number of sites. As a matter of fact, our algorithm for potential depending on shortest distances is slower than the use of nonpolar site−site diatomic potential but faster for more complex polyatomics. The inclusion of dipoles or charges has as practical consequence an increase of computational time for both kinds of potentials, but the same relation keeps for polar molecules. Computation of site−site correlation functions can also be implemented in our algorithm at a negligible computational cost.[22,29] In spite of its simplicity, coarse-grained models considering algorithms close to ours have been successfully used in very different fields.[30–35]

Moreover, the dipolar interaction is given by

$$u^{\mu\mu} = \frac{\boldsymbol{\mu}_1\boldsymbol{\mu}_2}{r^3} - \frac{3(\boldsymbol{\mu}_1 r)(\mu_2 r)}{r^5} \quad (3)$$

The vector $\boldsymbol{\mu}$ is directed along the line defined by the rod for the axial dipole and has a modulus μ. This dipole may be shifted from the center of the rod a length λL. If $\lambda = 0$ the dipole is placed on the center of the rod and if $\lambda = 0.5$, the dipole is at the extreme of the rod. In addition, the dipole can be rotated an angle χ with respect to the molecular axis as shown in Figure 1. Our new model includes two new parameters λ and χ whose physical meaning is well established. Moreover, we define the symbols $L^* = L/\sigma$ and $\mu^{*2} = \mu^2/(\varepsilon\sigma^3)$.

TABLE 1: Critical Properties of Different Linear Kihara Dipolar Models

	L^*	μ^{*2}	λ	χ	T_c^*	n_c^*	p_c^*
model 1	0.3	0	0	0	1.114_{12}	0.219_6	0.07_1
model 2	0.3	1.5	0	0	1.21_4	0.22_2	0.07_2
model 3	0.3	3	0	0	1.36_5	0.206_{13}	0.065_{15}
model 4	0.6	0	0	0	1.000_{12}	0.161_5	0.05_1
model 5	0.6	2	0	0	1.09_3	0.17_1	0.050_{15}
model 6	0.6	4	0	0	1.22_2	0.16_2	0.047_{13}
model 7	0.6	4	0.25	0	1.33_9	0.15_3	0.05_4
model 8	0.6	4	0.5	0	1.30_4	0.16_3	0.052_2
model 9	0.6	4	0	70.5	1.364_9	0.163_8	0.0519_1
model 10	0.6	4	0.5	70.5	1.432_6	0.153_2	0.05_1
model 11	0.8	0	0	0	0.95_1	0.140_3	0.038_8
model 12	0.8	2.3	0	0	1.03_2	0.143_{15}	0.037_7
model 13	0.8	4.6	0	0	1.18_4	0.137_{13}	0.038_{13}
model 14	0.8	4	0	0	1.127_8	0.128_{15}	0.03_2
model 15	0.8	4	0.25	0	1.20_2	0.130_8	0.04_2
model 16	0.8	4	1	0	1.3_1	0.13_5	0.031_{15}
model 17	0.8	1.5	0.5	70.5	1.05_3	0.145_{14}	0.044_7
model 18	1	2.5	0	0	0.994_{25}	0.12_9	0.034_9
model 19	1	2.5	0.5	70.5	1.11_2	0.125_{12}	0.038_7
model 20	1	2.5	0.25	0	0.99_4	0.113_{21}	0.02_2
model 21	1	2.5	0.5	0	1.0_1	0.12_5	0.03_3
model 22	2	1	0.5	0	0.81_3	0.07_2	0.016_5

We have performed simulations for the models presented in Table 1 using GEMC using a total number of 512 particles. Figure 2 shows the vapor−liquid equilibrium (VLE) curves for models with $L^* = 0.6$ and $\mu^{*2} = 4$ with different shifts and tilt angles with respect to the molecular axis. It is quite apparent that either the displacement of the dipole out of the molecular center or the tilt of the dipole respect to the molecule axis have an important influence on the VLE. In general, any of these changes in the dipole leads to an increase in the reduced critical temperature, $T^* = T/(\varepsilon/k_B)$, while the critical density is not so sensitive. Compressibility factor suffers a clear increase when the dipole is shifted to the extreme for axial dipole but only a

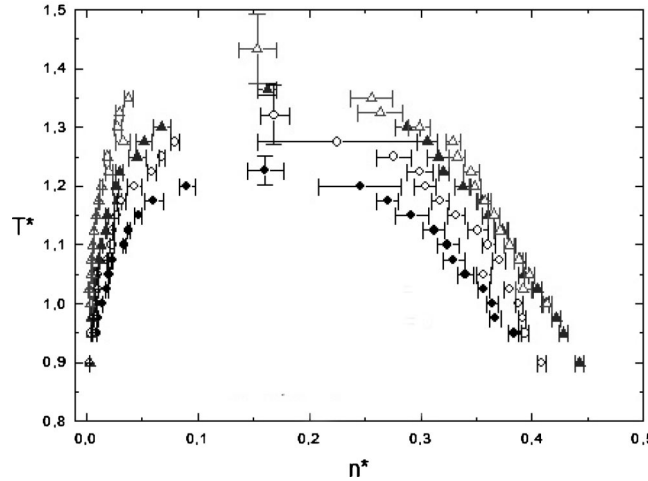

Figure 2. Vapor−liquid coexistence properties of some of the models with $L^* = 0.6$ and $\mu^{*2} = 4$. (●, $\lambda = 0$, $\chi = 0$; ○, $\lambda = 0.5$, $\chi = 0$; ▲, $\lambda = 0$, $\chi = 70.5$; △, $\lambda = 0.5$, $\chi = 70.5$).

slight decrease for the system with rotated dipole. All the values for critical properties of models are also shown in Table 1.The qualitative variation with the displacement of the dipole along the molecular axis is in agreement with the previously published results for longer rods and higher dipoles.[10]

Simulations were carried out in the Gibbs ensemble using the method proposed by Panagiotopoulos[36] and broadly used by ourselves.[4,37–39] This method enables the determination of coexistence densities at a given temperature in only one run. We have used 512 particles with 256 in each box. Initial molecular configuration was taken as corresponding either to an α-N_2 lattice or to the output of a close equilibrium state. Each GEMC simulation run yields reduced densities $n^* = n\sigma^3$ (both in gas and liquid phases) at the reduced pressure $p^* = p\sigma^3/\varepsilon$ at a fixed reduced temperature $T^* = T/(\varepsilon/k_B)$, where k_B is the Boltzmann constant. Several simulations were performed for elongations $L^* = L/\sigma$ varying from 0 to 2 and dipole moments $\mu^{*2} = \mu^2/(\varepsilon\sigma^3)$ ranging from 0 to 4. We used about 3 × 10^3 cycles to equilibrate and 2 × 10^3 to evaluate averages. Long-range electrostatic contributions were treated in a reaction field formalism with $\varepsilon_{RF} = \infty$. When T^* is near the critical point, liquid and gas boxes easily interchange and simulation is not possible. However this point can be extrapolated using the rectilinear diameter law

$$\frac{n_l^* + n_g^*}{2} = a + bT^* \tag{4}$$

and the critical exponent law

$$n_l^* - n_g^* = c\left(1 - \frac{T}{T_c}\right)^{\beta} \tag{5}$$

where the exponent β is chosen to be $^1/_3$, close to the critical exponent determined by experiment or from renormalization group theory.

Equations 4 and 5 can be rewritten as

$$(n_l^* - n_g^*)^3 = f - gT^* \tag{6}$$

Moreover, vapor pressure can be fitted to a Clausius−Clapeyron law

$$\ln p^* = d - \frac{e}{T^*} \tag{7}$$

The simulation fitting parameters can easily be associated with experimental parameters. So, reduced critical variables can be written as

$$T_c^* = \frac{f}{g} \tag{8}$$

$$n_c^* = a + bT_c^* \tag{9}$$

$$p_c^* = \exp(d - \frac{e}{T_c^*}) \tag{10}$$

because liquid and gas densities are the same at the critical point. The corresponding absolute values of these properties are now equated to the experimental points as:

$$T_c^{GEMC} = T_c^{exp} \tag{11}$$

$$n_c^{GEMC} = n_c^{exp} \tag{12}$$

and potential parameters can be obtained from

$$\varepsilon/k_B = (\frac{T_c^{exp}}{T_c^*}) \tag{13}$$

$$\sigma = \left(\frac{10000 n_c^*}{6.023 n_c^{exp}}\right)^{1/3} \tag{14}$$

$$\mu^{*2} = \frac{\mu^2}{\varepsilon\sigma^3} \tag{15}$$

From these results, we can also determine vaporization enthalpy ΔH_v, critical compressibility factor Z_c, the acentric factor ω, and the Hildebrand solubility parameter δ

$$\frac{d\ln p}{d(1/T)} = \frac{\Delta H_v}{RT^2} \tag{16}$$

$$Z_c = \frac{p_c}{RT_c\rho_c} \tag{17}$$

$$\omega = \log\left(\frac{p_c}{p}\right)_{T=0.7T_c} - 1 \tag{18}$$

$$\delta = \left(\frac{\Delta H_v - RT}{V}\right)^{1/2} \tag{19}$$

In the definition of δ the vaporization enthalpy is written in cal/mol and the molar volume V in mL/mol.

Finally, we must add that after this fitting we allowed in some cases for small variation of parameter ϵ to obtain a better overall agreement at the cost of slight differences in the critical temperature of the fitted model and the experiment (see Table 2).

III. Simulation Results and Comparison with the Experiment

III.1. Models. Table 1 shows the effect of nonaxiality and nonalignment of the dipole with respect to the center of mass. It can be observed that the inclusion of these parameters acts in a similar way than the multipolar interaction, i.e., both the factors lead to increased values of critical properties, especially the critical temperature. This effect is more noticeable on temperature when the dipole is displaced and tilted (model 4) but weaker on pressure and density. The effect on these last properties is mostly influenced by the displacement of the dipole. VLE curves and a Clausius plot are shown in Figures 2 and 3.

III.2. Real Substances. ***III.2.1. Amines.*** The wide set of models shown in Table 1 has been fitted to experimental data of 1-amines. As can be seen in Table 2 and Figures 4 and 5, our results show a general improvement with respect to the models previously proposed for small amines in which the dipole was centered on the molecule.[4] Agreement is of the same quality or slightly better than that obtained from more complicate intermolecular potentials.[2] A similar agreement between simulation and experiment is found for long-chain amines that have not been modeled previously. Note that agreement is particularly impressive for vapor pressure where our simulations match very well the experiment for several orders of magnitude. The results are remarkably good taking into account that amines form hydrogen bonds which are not considered explicitly in the model. Moreover, we have found that $\varepsilon = 84.695 \ln n_c + 328.76$ and $\sigma = 0.2793 n_c + 2.8705$ where n_c is the number of carbon atoms. Thus, potential parameters are transferable among amines.

III.2.2. Acetonitrile. Results for equilibrium properties of acetonitrile can be observed in Figure 6. Our results are of

TABLE 2: Molecular Parameters and Properties Estimation for 1-Amines (Comparison with Previous Results Included)

		CH_3NH_2	$CH_3CH_2NH_2$	$CH_3CH_2CH_2NH_2$	$CH_3(CH_2)_3NH_2$	CH_3NHCH_3
T_c (K)	exptl	430.05	456.15	496.95	524.15	437.7
	GEMC	430.05	457.39	502.941	524.197	437.7
ρ_c (mol/L)		8.33	5.49	4	3.45	5.35
L^*		0.6	0.8	0.8	0.8	0.8
λ		0.25	0.25	0.25	0.25	0.25
μ^{*2}		4	4	4	4	4
ϵ/k_B		328.230	387	425.5	443.483	370.295
σ (Å)		3.146	3.419	3.74	3.97	3.439
p_c (bar)	exptl	74.6	56.2	47.4	42	53.1
	GEMC	67.09	53.66	45.10	36.86	50.46
	prev	83.7	49.5			
μ (D)	exptl	1.31	1.22	1.17	0.99/1.4	1.03
	MC	2.38	2.922	3.506	3.915	2.88
	prev	2.99	3.2			
T_b (K)	exptl	266.82	289.7	321.65	351	281.1
	GEMC	252.39	285.1	318.54	336.504	274.40
	prev	237	287			
ΔH_v^0 (kJ/mol)	exptl	24.3	26.6	31.3	35.71	25.4
	GEMC	24.98	25.93	28.44	29.72	24.76
ω	exptl	0.281/0.292	0.285	0.28/0.303	0.397/0.33	
	MC	0.118	0.231	0.236	0.203	0.23
	prev	0.22	0.23			
Z_c	exptl	0.321	0.307	0.298	0.294	0.273
	GEMC	0.225	0.256	0.259	0.245	0.259
	prev	0.28	0.24			
δ	exptl	11.2	10.0			
	MC	17	14.23	13.08	12.25	13.74
	prev	9.4	9.8			

similar accuracy than previous models including simultaneous dipole and quadrupole contributions centered on the rod[40] with respect to VLE and vapor saturation pressure. This fact suggests that the inclusion of an out-of-the-center dipole regarding to the chemical intuition can implicitly take into account quadrupolar effects on thermodynamics. The next step is to develop molecular dynamics simulations in order to prove if this model is good enough to reproduce dynamical properties of this molecule, such as diffusion coefficient or shear viscosity.

III.2.3. 1-Alcohols. The application of the models to *n*-alcohols turns out much more complicated. Although the model reproduced quite well the VLE diagram (Figure 7) with a similar accurateness than more complicated intermolecular potentials,[41] computed saturation pressure (see Figure 8) is only accurate enough in a temperature range close to room temperature. The fact that the dipole moment experimentally measured used to be lesser than the calculated by simulation is a sign of the important role of hydrogen bonds formed by these molecules in the liquid state. So, neither enthalpy nor pressure are expected to be accurately foreseen from our model. However, it is apparent from Figures 7 and 8 that the agreement increases with the chain length and results are particularly good for 1-octanol that is an important molecule as we point out in the introduction. As expected, the larger the molecular volume, the less the relative weight of the hydrogen bond in the total intermolecular energy and our model works better for long chains.

III.2.4. α,ω-Diols. An important feature of our model is that it predicts the appearance of dimers for relatively long rods and dipoles rather shifted to the extreme. This dimer is predicted to appear at values of $\lambda \approx 0.42$ or higher.[14] That corresponds to the models for alcohols but not for amines as it is shown in Tables 2 and 4. In the case of diols, such a pairing would yield a dimer that, considered as a whole, possesses a quadrupole but not a dipole. So, we can expect that a simple quadrupole

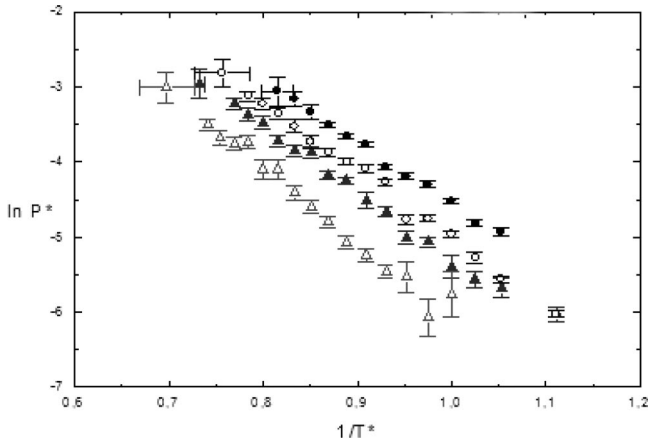

Figure 3. Vapor pressure vs inverse temperature of models in Figure 2.

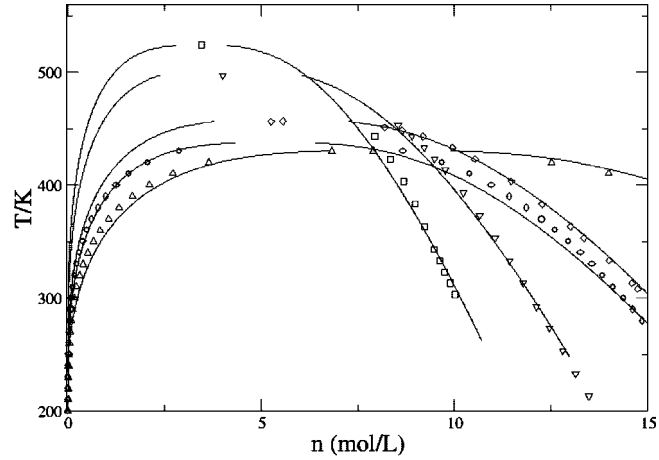

Figure 4. Vapor−liquid coexistence densities for amines. Symbols are experimental data, and solid lines are predictions using models defined in Table 2. Δ, methylamine; ○, DMA; ◇, ethylamine; ▽, propilamine; □, butilamine.

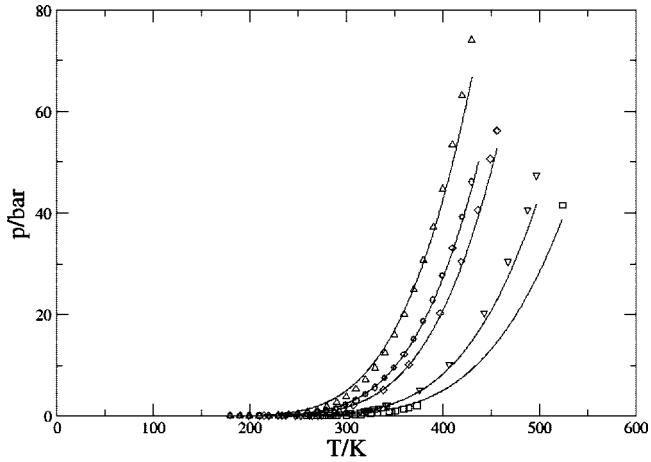

Figure 5. Clausius plot for *n*-amines. Symbols and lines as in Figure 4.

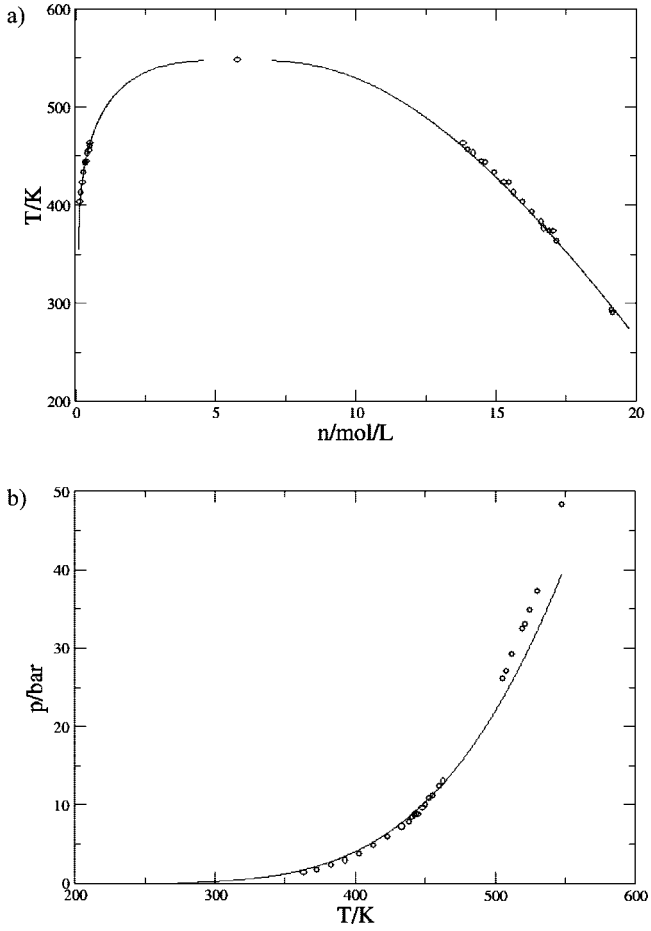

Figure 6. (a) Vapor−liquid coexistence densities for acetonitrile. Symbols are experimental data, and solid lines are predictions using models defined in Table 3. (b) Clausius plot for acetonitrile. Symbols and lines as in Figure 4.

model can give better results than any dipolar model. Therefore, we performed some ab initio calculations for long-chain α,ω-diols using a HF/6-311G* method/basis set.[42] Our results indicate that this kind of molecules can form dimers for a number of carbon atoms higher than 4. For less carbon atoms dimers are not stable, probably due to a steric repulsion and they form chains. We have tried to fit quadrupolar models to 1,4-butanediol where a few experimental results are available.[43,44] The new results move one step in the right direction, and they are certainly promising as shown in Figure 9. Note that the best

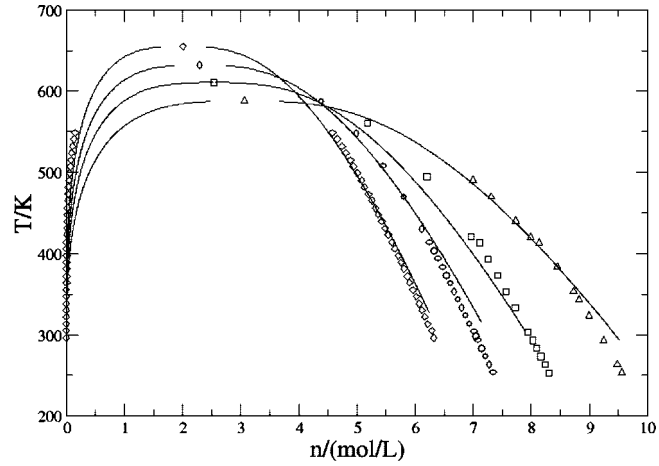

Figure 7. Vapor−liquid coexistence densities for long chain alcohols Symbols are experimental data, and solid lines are predictions using models defined in Table 4. Δ, octanol; ○, heptanol; □, hexanol; ◊, pentanol.

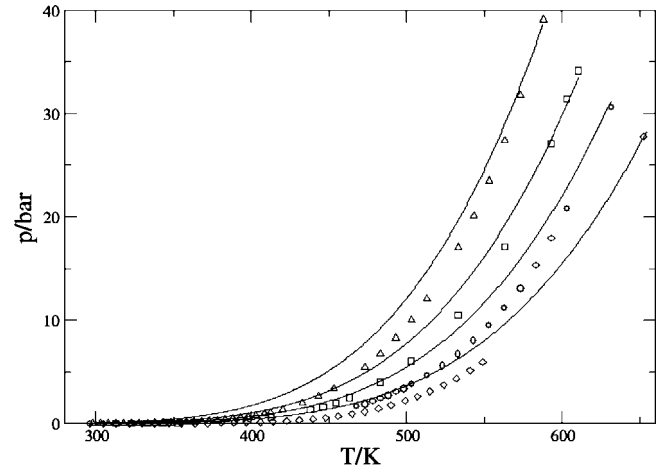

Figure 8. Clausius plot for long chain alcohols. Symbols and lines as in Figure 2.

TABLE 3: Molecular Parameters and Properties Estimation for Acetonitrile with the Model Presented in this Work (M3) (Comparison with Previous Models (M1 and M2) Is Included)

CH_3CN	exptl	M1	M2	M3
T_c (K)	547.85	547.85	547.85	547.85
ρ_c (mol/L)	5.77	5.77	5.77	5.77
L^*		0.8	0.8	0.6
λ		0	0	0.5
μ^{*2}		8	6	4
Q^{*2}		1	4	0
ϵ/k_B		357.42	307.35	382.010
σ(Å)		3.318	3.456	3.484
p_c(bar)	48.3	56.3	50.98	39.59
μ (D)	3.92	3.80	3.24	2.987
T_b (K)	354.8	367		342.95
ΔH_v (kJ/mol)	33.4	28.7	27.0	28.67
ω	0.327			0.168
Z_c	0.253	0.215	0.1642	0.1514
δ	12.1		12.5	15.7

fit corresponds to a value of $L^* = 0.3$, which is about half the size of a monomer, which means double thickness and the same length according to the definition of L^*. We are aware of some experiments on α,ω-diols ranging from 1,5-pentanediol to 1,8-octanediol[45] but they are not yet available, and we could not compare directly.

TABLE 4: Molecular Parameters and Properties Estimation for Long-Chain 1-Alcohols

	$CH_3(CH_2)_4OH$	$CH_3(CH_2)_5OH$	$CH_3(CH_2)_6OH$	$CH_3(CH_2)_7OH$
T_c (K)	586.15	610.15	631.9	652.2
ρ_c (mol/L)	3.063	2.62	2.3	2.04
L^*	0.8	0.8	0.8	0.8
λ	0.5	0.5	0.5	0.5
μ^{*2}	4	4	4	4
ϵ/k_B	448.221	516.54	534.65	554.194
σ(Å)	4.392	4.409	4.56	4.77
p_c (bar) exptl	38.9	34.1	30.58	27.77
p_c (bar) MC	28.48	32.44	30.36	27.49
μ (D) exptl	1.7	1.65	1.67	1.65
μ (D) MC	4.57	4.94	5.29	5.75
T_b (K) exptl	410.95	430.15	449.4	468.35
T_b (K) MC	369.946	589.13	614.21	642.55
ΔH_v (kJ/mol) exptl	55.56	62.8	66.94	70.96
ΔH_v (kJ/mol) MC	29.07	34.55	35.76	37.07
ω exptl	0.579	0.575	0.567	0.582/0.594
ω MC	1.59	1.73	1.74	1.77
δ MC	10.4	11.4	11.00	11.48

IV. Conclusions

The new model presented in this work shows a definite improvement on the agreement between simulation and experiment with respect to the thermodynamic properties over previous ones. Note that this model includes new parameters (λ and χ), but they are not simply fitting parameters because they own a deep physical meaning. So, this model is closer to the chemical intuition because dipoles are shifted to an extreme where the most electronegative atom lies. The tilt of the dipole has also a clear physical meaning because the dipole moment vector is directed along the more polar bond in the molecule. Thus, it is not necessary to include more terms in the multipole expansion of the charge distribution because the convergence is faster. All these models are in addition supported by quantum chemistry calculations. Indeed, geometrical center and center of charges are clearly separated in amines, and our quantum calculations yield values of λ between 0.2 and 0.35, in agreement with our models. Furthermore, amines and acetonitrile have high dipole moments, very high in the case of acetonitrile, in very good to excellent agreement with our models. Agreement for alcohols is not so satisfactory in spite of the experimental values of dipole moment for alcohols being similar to those of amines. This discrepancy can be attributed to very strong directional forces as hydrogen bonds that are not explicitly considered in our model. The possibility of the apparition of dimers is one of the advantages of our model, and this fact is here applied to α,ω-diols where dimers can be formed through pairing compensating dipoles. In this way, each molecule can act as a donor and an acceptor in the hydrogen bonds. Results considering dimers as a whole move in the right direction but more experiments would be necessary to validate this conclusion. Finally, we can conclude from the vicinity of δ-solubility parameter, calculated at 298.15 K, of all the substances that the mutual solubility should be very high in agreement with common experience.

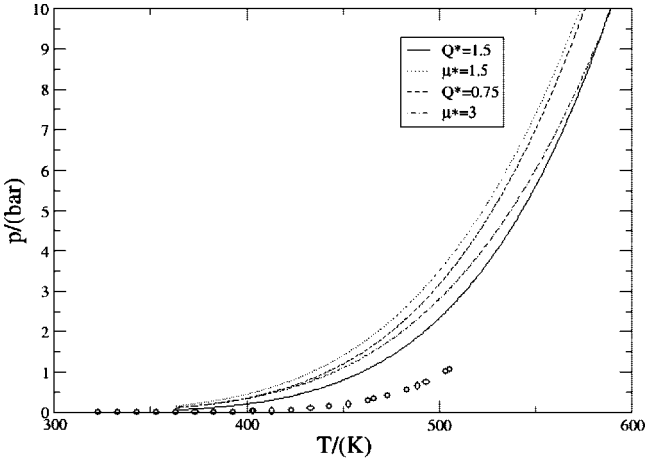

Figure 9. Estimated saturation pressure for 1,4-butanediol for a quadrupolar model of $L^* = 0.3$ and two different quadrupole moment.

Acknowledgment. This work was supported by Grants CTQ2007-60930 and BFM2003-07055. M.C. wishes to thank the Spanish Ministerio de Educación y Ciencia for a postgraduate fellowship.

References and Notes

(1) *Molecular Simulation and Industrial applications, Methods, examples and prospects*; Gubbins, K. E.,. Quirke, N. Eds.; Gordon and Breach: Amsterdam, 1996.
(2) Wick, C. D.; Stubbs, J. M.; Rai, N.; Siepmann, J. I. *J. Phys. Chem. B* **2005**, *109*, 18974.
(3) Garzón, B.; Lago, S.; Vega, C.; Rull, L. F. *J. Chem. Phys.* **1995**, *102*, 7204–7216.
(4) Lago, S.; Garzón, B.; Calero, S.; Vega, C. *J. Phys. Chem.* **1997**, *101*, 6763–6771.
(5) Stoll, J.; Vrabec, J.; Hasse, H. *J. Chem. Phys.* **2003**, *119*, 11396–11407.
(6) Stoll, J.; Vrabec, J.; Hasse, H. *Fluid Phase Equilib.* **2003**, *209*, 29–53.
(7) Bauergogonea, S.; Bauer, S.; Wirges, W.; Gerhardmulthaupt, R. *J. Appl. Phys.* **1994**, *76*, 2627–2635.
(8) Ha, T.; Laurence, T. A.; Chemla, D. S.; Weiss, S. *J. Phys. Chem. B* **1999**, *103*, 6839–6850.
(9) Weston, K. D.; Goldner, L. S. *J. Phys. Chem. B* **2001**, *105*, 3453–3462.
(10) Calero, S.; Lago, S.; Garzón, B. *Mol. Sim.* **2003**, *29*, 519–525.
(11) Debarre, A.; Jaffiol, R.; Julien, C.; Nutarelli, D.; Richard, A.; Tchenio, P.; Chaput, F. *Boilot J.P. Eur. Phys.J. D* **2004**, *28*, 67–77.
(12) Yang, J.; Winnik, M. A.; Pakula, T. *Macromolecules* **2005**, *38*, 8882–8890.
(13) Hohlbein, J.; Hubner, C. G. *Appl. Phys. Lett.* **2005**, *86*, 121104.
(14) Lago, S.; López-Vidal, S.; Garzón, B.; Mejías, J. A.; Anta, J. A.; Calero, S. *Phys. Rev. E* **2003**, *68*, 1–4.
(15) Lipinski, C.; Lombardo, F.; Dominy, B. W.; Feeney, P. J. *Adv. Drug Del. Rev.* **1997**, *23*, 3–25.
(16) Jorgensen, W. L.; Duffy, E. M. *Bioorg. Med. Chem. Lett.* **2000**, *10*, 1155–1158.
(17) Curutchet, C.; Orozco, M.; Luque, F. J. *J. Comput. Chem.* **2001**, *22*, 1180–1193.
(18) Banerjee, S.; Yalkowsky, S. H.; Valvani, S. C. *Env. Sci. Technol.* **1980**, *14*, 1227–1229.

(19) Klotz, W. L.; Schure, M. R.; Foley, J. P. *J. Chromatogr. A* **2001**, *930*, 145–154.

(20) Fisk, A. T.; Hobson, K. A.; Norstrom, R. J. *Env. Sci. Technol.* **2001**, *35* (4), 732–738.

(21) Vega, C.; Lago, S. *J. Chem. Phys.* **1990**, *93*, 8171–8179.

(22) Calero, S.; Garzón, B.; Mejías, J. A.; Lago, S. *J. Chem. Phys.* **2001**, *114*, 9075–9082.

(23) Vega, C.; Lago, S.; Pospisil, R.; Labik, S.; Malijevski, A. *J. Phys. Chem.* **1992**, *96*, 1895.

(24) Sevilla, P.; Lago, S. *Comput. Chem.* **1985**, *9*, 39–42.

(25) Lago, S.; Vega, C. *Comput. Chem.* **1988**, *12*, 343–356.

(26) Vega, C.; Lago, S. *Comput. Chem.* **1994**, *18*, 55–59.

(27) Boublík, T. *Mol. Phys.* **1992**, *76*, 237.

(28) Vesely, F. *J. Chem. Phys.* **2006**, *125*, 214106.

(29) Cortada, M.; Calero, S.; Lago, S. *J. Chem. Phys.* **2005**, *123*, 1–10, 184502.

(30) Janecek, J.; Boublik, T. *Mol. Phys.* **2006**, *104*, 197.

(31) Brannigan, G.; Brown, F. L. H. *J. Chem. Phys.* **2004**, *120*, 1059.

(32) Abreu CRA, Tavares FW, Castier M, Powder Tech, 134, 167, 2003.

(33) Varga, S.; Jackson, G. *Mol. Phys.* **2006**, *104*, 368.

(34) Almohamad, H. A. *Arabian J. Sci. Eng.* **1998**, *23*, 243–251.

(35) Vega, C.; Gubbins, K. E. *Mol. Phys.* **1992**, *75*, 881.

(36) Panagiotopoulos, A. Z. *Mol. Phys.* **1987**, *61*, 813.

(37) Vega, C.; Lago, S.; de Miguel, E.; Rull, L. F. *J. Phys. Chem.* **1992**, *96*, 7431–7437.

(38) Garzón, B.; Lago, S.; Vega, C.; de Miguel, E.; Rull, L. F. *J. Chem. Phys.* **1994**, *101*, 4166–4176.

(39) Garzón, B.; Lago, S.; Vega, C.; Rull, L. F. *J. Chem. Phys.* **1995**, *102*, 7204–7216.

(40) Calero, S.; Garzón, B.; MacDowell, L. G.; Lago, S. *J. Chem. Phys.* **1997**, *107*, 2034–2045.

(41) Khare, R.; Sum, A. K.; Nath, S. K.; de Pablo, J. J. *J. Phys. Chem. B* **2004**, *108*, 10071.

(42) Frisch, M. J.; Trucks, G. W.; Schlegel, H. B.; Scuseria, G. E.; Robb, M. A.; Cheeseman, J. R.; Montgomery, J. A., Jr.; Vreven, T.; Kudin, K. N.; Burant, J. C.; Millam, J. M.; Iyengar, S. S.; Tomasi, J.; Barone, V.; Mennucci, B.; Cossi, M.; Scalmani, G.; Rega, N.; Petersson, G. A.; Nakatsuji, H.; Hada, M.; Ehara, M.; Toyota, K.; Fukuda, R.; Hasegawa, J.; Ishida, M.; Nakajima, T.; Honda, Y.; Kitao, O.; Nakai, H.; Klene, M.; Li, X.; Knox, J. E.; Hratchian, H. P.; Cross, J. B.; Bakken, V.; Adamo, C.; Jaramillo, J.; Gomperts, R.; Stratmann, R. E.; Yazyev, O.; Austin, A. J.; Cammi, R.; Pomelli, C.; Ochterski, J. W.; Ayala, P. Y.; Morokuma, K.; Voth, G. A.; Salvador, P.; Dannenberg, J. J.; Zakrzewski, V. G.; Dapprich, S.; Daniels, A. D.; Strain, M. C.; Farkas, O.; Malick, D. K.; Rabuck, A. D.; Raghavachari, K.; Foresman, J. B.; Ortiz, J. V.; Cui, Q.; Baboul, A. G.; Clifford, S.; Cioslowski, J.; Stefanov, B. B.; Liu, G.; Liashenko, A.; Piskorz, P.; Komaromi, I.; Martin, R. L.; Fox, D. J.; Keith, T.; Al-Laham, M. A.; Peng, C. Y.; Nanayakkara, A.; Challacombe, M.; Gill, P. M. W.; Johnson, B.; Chen, W.; Wong, M. W.; Gonzalez, C.; Pople, J. A. *Gaussian 03*, revision C.02; Gaussian, Inc.: Wallingford, CT, 2004.

(43) Alexander A:L., Stevens C. L., McCrone W. C., Watt G. W. *Physical properties of Chemical Compounds*; American Chemical Society: 1955.

(44) Timmermans J. *Physicochemical constants of pure organic compounds*: Elsevier, 1965.

(45) Kimura, T.; Inui, S.; Kamiyama, T. Poster presented at 19th International Conference on Chemical Thermodynamics, Boulder, Colorado, USA, August 2006.

JP801680Z